

# Temperature gradient driven heat flux closure in fluid simulations of collisionless reconnection

F. Allmann-Rahn<sup>1</sup>, T. Trost<sup>1</sup> and R. Grauer<sup>1†</sup>

<sup>1</sup>Institute for Theoretical Physics I, Ruhr University Bochum, Germany

(Received xx; revised xx; accepted xx)

Recent efforts to include kinetic effects in fluid simulations of plasmas have been very promising. Concerning collisionless magnetic reconnection, it has been found before that damping of the pressure tensor to isotropy leads to good agreement with kinetic runs in certain scenarios. An accurate representation of kinetic effects in reconnection was achieved in a study by Wang et al. (*Phys. Plasmas*, volume 22, 2015, 012108) with a closure derived from earlier work by Hammett and Perkins (*PRL*, volume 64, 1990, 3019). Here, their approach is analyzed on the basis of heat flux data from a Vlasov simulation. As a result, we propose a new local closure in which heat flux is driven by temperature gradients. That way, a more realistic approximation of Landau damping in the collisionless regime is achieved. Previous issues are addressed and the agreement with kinetic simulations in different reconnection setups is improved significantly. To the authors' knowledge, the new fluid model is the first to perform well in simulations of the coalescence of large magnetic islands.

## 1. Introduction

Magnetic reconnection is a process where magnetic field line topology changes (field lines reconnect) to an energetically more advantageous state. Magnetic energy is converted into heating and particle acceleration. Reconnection occurs throughout the universe, e.g. in the context of gamma ray bursts, in stellar and especially solar flares or in Earth's magnetosphere.

Plasma phenomena that happen on large time and spatial scales and those where collisions are an important factor can often be described sufficiently with hydrodynamic or fluid models. In many cases, such as collisionless magnetic reconnection and collisionless shocks, these conditions are not fulfilled and thus kinetic effects have to be taken into account. However, kinetic simulations are computationally expensive and problems with large system sizes like reconnection in the magnetotail or three-dimensional reconnection cannot be computed with a fully kinetic model. The fluid equations on the other hand can be orders of magnitude cheaper to compute and can be a good approximation depending on how well the corresponding closure suits the problem.

Wang *et al.* (2015) suggested a heat flux closure which approximates a spectrum of wave numbers by one single wave number  $k_0$ . The closure, although simple, gave very good results in fluid simulations of collisionless reconnection. Nevertheless, Wang et al. asserted that further work is needed to improve the closure, e.g. by finding a more suitable  $k_0$ . One way to do this is to compare the closure approximation to the actual heat flux gained from a kinetic simulation. This is difficult with a particle in cell (PIC) code because

† Email address for correspondence: grauer@tp1.rub.de

higher moments like pressure and especially heat flux are very noisy in PIC simulations. We analyze the closure making use of kinetic data from a Vlasov simulation. Dependence of  $k_0$  on plasma parameters is sought as well as other major potential improvements to the closure.

## 2. Vlasov equation and ten moment fluid equations

A plasma may be described by distribution functions  $f_s(\mathbf{x}, \mathbf{v}, t)$  which determine the particle density at point  $(\mathbf{x}, \mathbf{v})$  in phase space at time  $t$  for the particle species  $s$ . Under the assumption that there are no collisions (which is a good approximation e.g. for plasmas in space physics), the evolution of the distribution function is given by the continuity equation

$$\frac{\partial f_s}{\partial t} + \nabla \cdot (\mathbf{v} f_s) + \nabla_v \cdot (\mathbf{a} f_s) = 0. \quad (2.1)$$

Inserting Lorentz acceleration  $\mathbf{a} = \frac{q}{m}(\mathbf{E} + \mathbf{v} \times \mathbf{B})$ , the equation can be rearranged to give the **Vlasov equation**

$$\frac{\partial f_s}{\partial t} + \mathbf{v} \cdot \nabla f_s + \frac{q_s}{m_s}(\mathbf{E} + \mathbf{v} \times \mathbf{B}) \cdot \nabla_v f_s = 0. \quad (2.2)$$

Evolution of electric and magnetic fields is given by Maxwell's equations  $\nabla \cdot \mathbf{E} = \frac{\rho}{\epsilon_0}$ ,  $\nabla \cdot \mathbf{B} = 0$ ,  $\nabla \times \mathbf{E} = -\frac{\partial \mathbf{B}}{\partial t}$  and  $\nabla \times \mathbf{B} = \mu_0 \mathbf{j} + \mu_0 \epsilon_0 \frac{\partial \mathbf{E}}{\partial t}$ .

The charge and current densities are defined as  $\rho = \sum_s q_s n_s$  and  $\mathbf{j} = \sum_s q_s \mathbf{u}_s$ . Fluid quantities can be derived by taking moments of the distribution function, i.e. multiplying  $f_s$  by powers of  $v$  and taking the integral over velocity space. The zeroth moment is the particle density  $n_s(\mathbf{x}, t) = \int f_s(\mathbf{x}, \mathbf{v}, t) d\mathbf{v}$ . Similarly, the first moment is the mean velocity  $\mathbf{u}_s(\mathbf{x}, t) = \frac{1}{n_s(\mathbf{x}, t)} \int \mathbf{v} f_s(\mathbf{x}, \mathbf{v}, t) d\mathbf{v}$ . Higher moments include pressure  $P_s = m_s \int \mathbf{v}' \otimes \mathbf{v}' f_s d\mathbf{v}$  and heat flux  $Q_s = \frac{m_s}{2} \int \mathbf{v}' \otimes \mathbf{v}' \otimes \mathbf{v}' f_s d\mathbf{v}$ , where  $\mathbf{v}' = \mathbf{v} - \mathbf{u}$ .

By taking moments of the whole Vlasov equation, one can obtain the fluid equations. Due to the  $\mathbf{v} \cdot \nabla f$  term in the Vlasov equation, however, every moment contains a quantity that is defined by the next higher moment. Therefore, the resulting system of equations needs a closure in order to be self consistent. Usually this is done by finding an approximation for pressure or heat flux. Two common versions of the fluid equations are the five moment equations (pressure closure) and ten moment equations (heat flux closure).

The following three equations along with Maxwell's equations and a heat flux closure are the complete set of **ten moment equations** ( $D$  denotes the dimensionality):

$$\frac{\partial n_s}{\partial t} + \nabla \cdot (n_s \mathbf{u}_s) = 0, \quad (2.3)$$

$$m_s n_s \left( \frac{\partial \mathbf{u}_s}{\partial t} + \mathbf{u}_s \cdot \nabla \mathbf{u}_s \right) = n_s q_s (\mathbf{E} + \mathbf{u}_s \times \mathbf{B}) - \nabla \cdot P_s, \quad (2.4)$$

$$\frac{D}{2} \left( \frac{\partial P_s}{\partial t} + \mathbf{u}_s \cdot \nabla P_s \right) + \frac{2+D}{2} P_s \nabla \cdot \mathbf{u}_s = -\nabla \cdot Q_s. \quad (2.5)$$

### 3. WHBG physical space fluid closure for Landau damping

Many heat flux closures for collisionless plasmas exist and have been successfully applied, e.g. the Landau damping closures by Hammett & Perkins (1990) or Passot & Sulem (2003). An overview is given in Chust & Belmont (2006). Most closures are not designed for heat flux and pressure tensors in three dimensions though. Hammett & Perkins (1990) (also: Hammett *et al.* (1992)) approximated the plasma response function using a Pade series in order to include Landau damping in the fluid equations which is the main damping mechanism – and thus cause of heat flux – in collisionless plasmas. The closure was found to be an excellent approximation in many different cases (see e.g. the study by Sarazin *et al.* (2009)).

The Hammett-Perkins closure is given in one-dimensional Fourier space as

$$\tilde{q}_k = -n_0 \chi_1 \frac{2^{1/2} v_t}{|k|} i k \tilde{T}_k \quad (3.1)$$

with  $v_t = \sqrt{k_B T / m}$  and  $\chi_1 = 2 / \sqrt{\pi}$ . The closure resembles Fick's second law  $q = -n D \frac{\partial T}{\partial x}$ .

It was found by Johnson & Rossmannith (2010) that heat flux in collisionless reconnection can be modeled by a relaxation of the pressure tensor to an isotropic equilibrium pressure. This can be motivated with the Hammett-Perkins closure: Eq. 3.1 was simplified by Wang *et al.* (2015) in order to be applicable in three dimensional physical space. Since  $\nabla \cdot \mathbf{Q}$  shall be approximated, the divergence of Eq. 3.1 is taken which gives

$$\text{LHS} = i \mathbf{k}^t \cdot \mathbf{Q}_s \quad (3.2)$$

on one side and

$$\text{RHS} = n_0 \chi_1 \frac{2^{1/2} v_t}{|k|} \mathbf{k}^t \cdot (\mathbf{k}^t \cdot \tilde{\mathbf{T}}_s) \quad (3.3)$$

on the other side of the equation. Here,  $\mathbf{k}^t$  is the transposed wave vector. It becomes obvious that a direct generalization of Fick's law to tensors is not possible since Eq. 3.2 is a second-order tensor and Eq. 3.3 is a scalar. Therefore, the vector character of  $\mathbf{k}$  was neglected on the right-hand side (and the constant  $\chi_1 \sqrt{2} \approx 1.6$  was dropped), resulting in

$$i k_m Q_{ijm}(k) \approx n_0 \frac{v_t}{|k|} k^2 \tilde{T}_{ij}(k) = n_0 v_t |k| \tilde{T}_{ij}(k). \quad (3.4)$$

The adjustment done by treating  $\mathbf{k}$  as a scalar is that (in physical space)  $\nabla \cdot (\nabla \cdot \mathbf{T}_s)$  is replaced by  $\nabla^2 \mathbf{T}_s$ , i.e. the Laplace operator is used on each component of  $\mathbf{T}_s$ . At the same time regular divergence is taken on the left-hand side. A motivation for this approximation is given in Sec. 7.

The perturbed temperature  $\tilde{T}_{ij}$  can be expressed as  $(P_{ij} - p \delta_{ij}) / n_0$ , where  $p \delta_{ij}$  is the isotropic pressure with  $p = (P_{xx} + P_{yy} + P_{zz}) / 3$ . Thus

$$i k_m Q_{ijm}(k) \approx v_t |k| (P_{ij}(k) - p(k) \delta_{ij}). \quad (3.5)$$

Finally, the wave number field  $k$  is approximated by one single wave number  $k_0$ , so that the closure can be written in physical space as

$$\partial_m Q_{ijm} \approx v_t |k_0| (P_{ij} - p \delta_{ij}). \quad (3.6)$$

We will refer to this closure as the scalar-k closure in this paper.

## 4. Numerical setup

Fluid and kinetic Vlasov simulations of different reconnection problems are performed. The Vlasov code is described in Schmitz & Grauer (2006*a,b*), the fluid code and its coupling to the Vlasov code is presented in Rieke *et al.* (2015). Time is normalized over inverse ion cyclotron frequency  $\Omega_{i,0}^{-1}$ , length over ion inertial length  $d_{i,0}$ , speed over Alfvén velocity  $v_{A,0}$  and mass over ion mass  $m_i$ . The electron-ion mass ratio is  $m_i/m_e = 25$  in all simulations.

### 4.1. GEM

The GEM (Geospace Environmental Modeling) reconnection setup (Birn *et al.* 2001) is a reconnection problem that uses a Harris sheet configuration (Harris 1962). The initial magnetic field is given by  $B_x(y) = B_0 \tanh(y/\lambda)$  and the particle density by  $n(y) = n_0 \operatorname{sech}^2(y/\lambda) + n_b$  where  $\lambda = 0.5$ ,  $B_0 = 1$ ,  $n_0 = 1$  and the background density  $n_b = 0.2$ . Temperature is defined by  $n_0(T_e + T_i) = B_0^2$ ,  $T_i/T_e = 5$ . Speed of light is set to  $c = 20 v_{A,0}$ . The domain is of size  $L_x \times L_y = (8\pi \times 4\pi) d_{i,0}$ . It is translationally symmetric in  $z$ -direction, periodic in  $x$ -direction and has conducting walls for fields and reflecting walls for particles in  $y$ -direction. In order to start the reconnection process, a perturbation in the magnetic field is applied that takes the form  $\mathbf{B} = \hat{\mathbf{z}} \times \nabla\psi$  where the perturbation in the magnetic flux is given by  $\psi(x, y) = 0.1 \cos(2\pi x/L_x) \cos(\pi y/L_y)$ . Because of symmetries, it is sufficient to simulate one fourth of the domain. The time span covered by the Vlasov simulation is  $40 \Omega_{i,0}^{-1}$ , reconnection rate peaks at  $t \approx 20 \Omega_{i,0}^{-1}$ . The domain is resolved by  $256 \times 128$  cells.

### 4.2. Large Harris sheet – WHBG

Reconnection in Earth’s magnetotail happens on much larger spatial scales than reconnection in the GEM setup. In order to approach larger scales, Wang *et al.* (2015) performed kinetic and fluid simulations in a configuration like GEM but with a  $(100 \times 50) d_{i,0}$  domain and  $c = 15 v_{A,0}$ . For simple reference, it will be called the WHBG setup in this paper. A study of reconnection in a domain of this size was done before by Daughton *et al.* (2006), but with open boundary conditions unlike the WHBG version.

### 4.3. Island coalescence

The island coalescence reconnection problem has also been studied extensively, e.g. by Karimabadi *et al.* (2011) (large PIC simulations), Stanier *et al.* (2015) (PIC, hybrid and Hall-MHD compared) and Ng *et al.* (2015) (MHD, Hall-MHD and ten moment fluid simulations). We use the same parameters as the aforementioned studies. The initial configuration is a Fadeev equilibrium (Fadeev *et al.* 1965):  $A_z = -\lambda B_0 \ln(\cosh(y/\lambda) + \epsilon \cos(x/\lambda))$  and  $n = n_0(1 - \epsilon^2)/(\cosh(y/\lambda) + \epsilon \cos(x/\lambda))^2 + n_b$  with  $\epsilon = 0.4$ ,  $n_b = 0.2$  and a variable  $\lambda$ . Temperature is  $T = T_i = T_e = 0.5$ , speed of light  $c = 15 v_{A,0}$  and the domain size is proportional to  $\lambda$  according to  $L_x \times L_y = (2\pi\lambda \times 4\pi\lambda) d_{i,0}$ . The boundaries are periodic in  $y$ -direction and conducting for fields and reflecting for particles in  $x$ -direction. The B-field perturbation is  $\delta B_x = 0.1 \sin(y/(2\lambda) - \pi) \cos(x/(2\lambda))$  and  $\delta B_y = -0.1 \cos(y/(2\lambda) - \pi) \sin(x/(2\lambda))$  (Daughton *et al.* 2009). Time is normalized to Alfvén time  $t_A = L_y/v_{A,0}$ . The normalized reconnection rate  $E_R$  is computed as  $E_R = \frac{\partial \psi}{\partial t} / (B' v'_A)$  where  $B'$  is the maximum of the absolute value of the magnetic field

between the X-point and the O-point at  $x = 0$  and  $t = 0$  and  $v'_A = B'/\sqrt{\mu_0 n_0 m_i}$ . The magnetic flux is  $\Psi = \int_{\text{O}}^{\text{X}} dy B_x$  (integral from the O- to the X-point).

## 5. Comparison of heat flux data and the scalar-k closure

In order to examine how well the actual divergence of heat flux agrees with the closure approximation, both sides of Eq. 3.6 have been computed. While Wang *et al.* chose  $1/d_{e,0}$  as  $k_0$  for all components, ideally one can find a better  $k_0$  by analyzing the plots (cf. Sec. 6) of the kinetic simulations. The comparison is done with simulations of the GEM setup.

Taking symmetry into account, the heat flux tensor  $Q_s$  has ten and the pressure tensor  $P_s$  has six independent components. Therefore Eq. 3.6 results in six separate equations, one for each of the pressure tensor's components.  $1/d_{e,0}$  equates to  $5 d_{i,0}^{-1}$  since the electron-ion mass ratio  $m_e/m_i$  is  $1/25$ . For the purpose of comparison, a value of  $k_0 = 1 d_{i,0}^{-1}$  is used to compute the closure. Representative plots are shown in Fig. 1.

Overall the agreement is decent considering that heat flux often has a complex shape. The approximation is best in the period before and during reconnection. In the beginning of the simulation the magnitude is usually off by a factor between  $\frac{1}{10}$  and 10 whereas after reconnection the shape of heat flux generally becomes very convoluted which is hard to replicate with a closure.

Fig. 1a shows typical issues insofar as the basic structure is approximated well (the area in the center of the plot) but other parts of the shape are wrong (here the outer area around the x-axis). Another recurring problem is that the whole outer region usually has no heat flux, which is wrongly predicted by the scalar-k closure. A major improvement with correct damping in this outer region will be presented in Sec. 7.

A positive example of the scalar-k closure is given by Fig. 1b, showing how it can even cover details like the changing sign at the left and right border around the x-axis. After reconnection, structures tend to get complicated (Fig. 1c) and while the shape is still similar, both sign and the location of extrema are inaccurate. This holds true for many components towards the end of the simulation (35 to 40  $\Omega_{i,0}^{-1}$ ). Concerning a fixed  $k_0$ , the comparison suggests that values between 0.1 and 10  $d_{i,0}^{-1}$  can be reasonable choices.

## 6. Searching for a parameter dependent $k_0$

The field of wave numbers  $k$  from Eq. 3.1 was replaced with a single fixed number  $k_0$  by Wang *et al.* (2015). Although this is a massive simplification, it already leads to good results. Nonetheless, there are differences between a kinetic simulation and a ten moment fluid simulation using the scalar- $k$  closure. Discrepancies exist e.g. in the pressure tensor which may be attributed to the issue that there is no trivial way to generalize the original Hammett-Perkins closure to three dimensions and that  $k$  is the same for each component of the pressure tensor.

The idea behind the approximation is that a  $k_0$  represents the average length scales at which Landau damping occurs in the given scenario. Wang *et al.* (2015) found  $k_0 = 1/d_{e,0} = 5 d_{i,0}^{-1}$  to fit well in their  $(100 \times 50)$   $d_{i,0}$  reconnection setup. Tests showed that in the original GEM reconnection problem, however,  $k_{0,i} = 0.3 d_{i,0}^{-1}$  seems to be the optimal value. This is unintuitive as usually a smaller domain size would not require a smaller (especially much smaller) characteristic wave number. That means  $k_0$  seems to

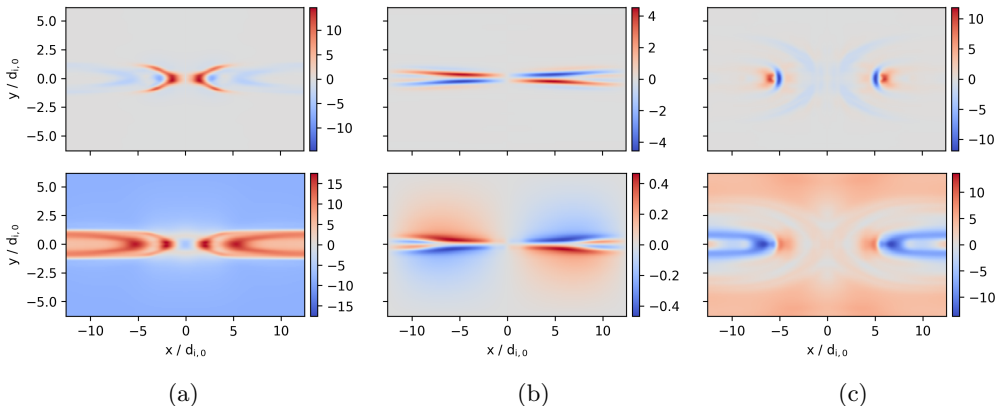


Figure 1: Comparison of actual heat flux change (first row) and scalar- $k$  closure (second row). (a)  $(\nabla \cdot \mathbf{Q}_e)_{xx}$  at  $t = 17.5 \Omega_i^{-1}$ , (b)  $(\nabla \cdot \mathbf{Q}_e)_{xy}$  at  $t = 7.5 \Omega_i^{-1}$ , (c)  $(\nabla \cdot \mathbf{Q}_e)_{zz}$  at  $t = 30 \Omega_i^{-1}$ .

be specific to the respective problem. It would be desirable to find a consistent, variable  $k_0$  which might depend on local plasma parameters.

Eligible plasma parameters were investigated experimentally by computing the closure with the respective  $k_0$  candidate and comparing it to the actual divergence of heat flux as done in Sec. 5. Promising candidates were additionally tested in a ten moment fluid simulation which was then compared to a run with  $k_0 = 5 d_{i,0}^{-1}$  and a Vlasov run. Dependence of  $k_0$  on plasma parameters and quantities was examined in the GEM setup, but none of the experiments lead to an improvement. This is because the closure's shape is overall decent and differences to the actual heat flux are often very complex or vary heavily in time and component. Results from the analysis done in Sec. 5 and in this section suggest that the deficiencies concerning shape and sign cannot be fixed with a scalar  $k_0$  dependent on plasma parameters. The same applies to the wrong magnitudes that appear early in the simulation because they don't relate to the fluid quantities.

## 7. Modified, gradient driven closure

The Hammett-Perkins closure was transferred to physical space because a Fourier space representation may be computationally expensive in a physical space code. More important is the issue that it is not clear how to generalize the closure to three-dimensional tensors. A generalization to tensors in Fourier space was proposed by Ng *et al.* (2017). They started with Eq. 3.1 and searched for a total symmetric generalisation of the heat flux  $Q_{ijm}$  resulting in

$$Q_{ijm}(\mathbf{x}) = n(\mathbf{x})\tilde{Q}_{ijm}(\mathbf{x}), \quad \hat{Q}_{ijm}(\mathbf{k}) = -i \frac{v_t}{|k|} \chi^k [i \hat{T}_{jk}], \quad (7.1)$$

where  $\hat{Q}_{ijm}$  and  $\hat{T}_{jk}$  denote the Fourier transforms of  $\tilde{Q}_{ijm}$  and  $T_{jk}$ .

We take a different approach and focus not on the heat flux directly but on its divergence  $\partial_m Q_{ijm}$ . To attain the symmetry of this divergence tensor, Wang *et al.* (2015) used  $-k^2 \mathbf{P}$  in place of the derivative  $-\mathbf{k}^t \cdot (\mathbf{k}^t \cdot \mathbf{P})$  and then approximated  $k$  by  $k_0$ . The physical space equivalent of this is to replace  $\nabla \cdot (\nabla \cdot \mathbf{P})$  by  $\nabla^2 \mathbf{P}$  where now the second approximation ( $k \approx k_0$ ) is not needed. This way the dependence on  $k_0$  is reduced and

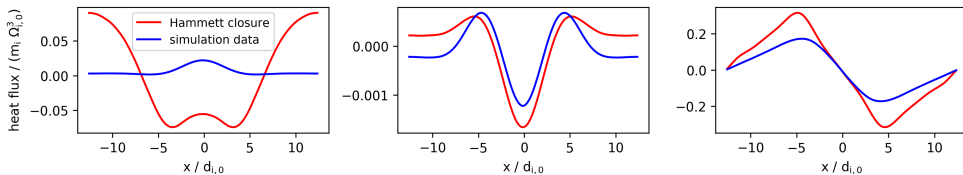


Figure 2: Hammett-Perkins closure, components from left to right:  $Q_{xxz,e}$ ,  $Q_{xxz,i}$ ,  $Q_{xyy,e}$ .

different relaxation in each component of the pressure tensor is allowed. The resulting expression takes the form of a Fick's law and thus the damping nature of the Hammett-Perkins closure is clearly retained.

Our candidate for a new collisionless heat flux closure is

$$\partial_m Q_{ijm} = -\frac{v_t}{|k_0|} \nabla^2 (P_{ij} - p\delta_{ij}), \quad (7.2)$$

where the symmetry of the divergence of the heat flux appears naturally. We will call it the gradient closure in this paper.

It is yet to be motivated why  $-k^2 P$  might be a suitable approximation of the derivative. In order to do so, assume  $\mathbf{B} = (B_x, 0, 0)$ . The wave vector  $\mathbf{k}$  is related to plasma oscillations, therefore  $\mathbf{k} \parallel \mathbf{B}$  and  $\mathbf{k} = (k_x, 0, 0)$ . The Hammett-Perkins closure in Wang et al.'s three-dimensional version is

$$ik_m Q_{ijm} = \chi_1 \frac{2^{1/2} v_t}{|k|} k^2 (P_{ij} - p\delta_{ij}) \quad (7.3)$$

or

$$ik_x Q_{ijx} + ik_y Q_{ijy} + ik_z Q_{ijz} = \chi_1 \frac{2^{1/2} v_t}{|k|} (k_x^2 + k_y^2 + k_z^2) (P_{ij} - p\delta_{ij}). \quad (7.4)$$

After dividing by  $ik_x$  and with  $k_y = k_z = 0$ , the equation has the form of the original Hammett-Perkins closure

$$Q_{ijx}(k) = -\chi_1 \frac{2^{1/2} v_t}{|k_x|} ik_x (P_{ij}(k) - p(k)\delta_{ij}). \quad (7.5)$$

Hence, Eq. 3.6 is a plausible generalization to three-dimensional tensors along magnetic field lines. This indicates that, while not exact in all space, the simplification of treating  $k$  as a scalar is reasonable.

In the outer region of the simulation, field lines are nearly parallel to the x-axis. Thus, it is straightforward to use Eq. 7.5 to test whether the Hammett-Perkins closure can be applied to the problem of reconnection or, more precisely, in how far the issues found are related to the choice of  $k_0$  and the scalar- $k$  approximation and in how far the problems are inherent to the original closure. The heat flux according to the closure was calculated by Fourier transforming a one-dimensional section of the pressure data with

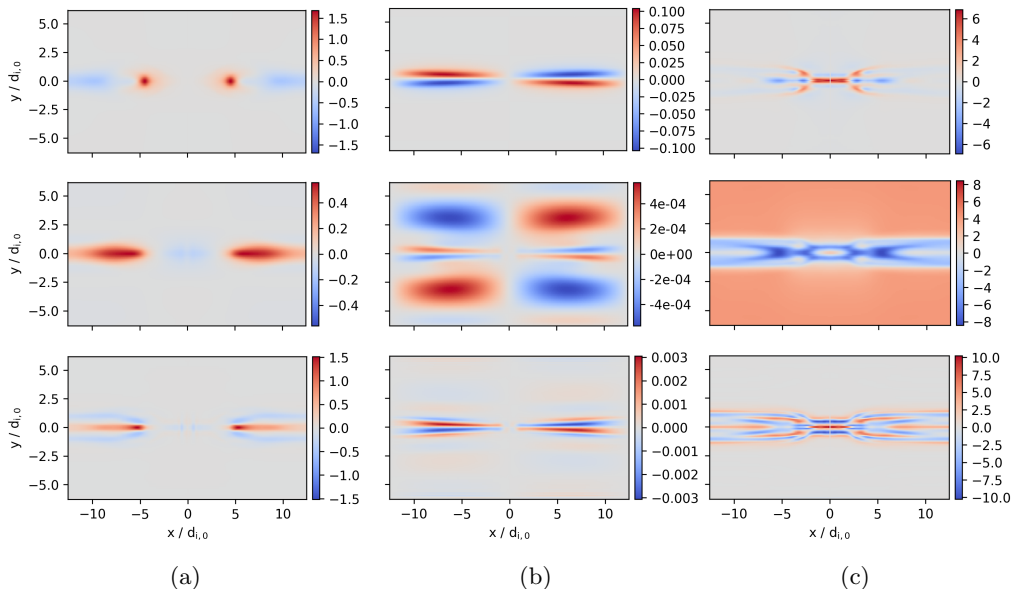


Figure 3: Comparison of actual heat flux change (first row), scalar- $k$  closure (second row) and gradient closure (third row). (a)  $(\nabla \cdot \mathbf{Q}_i)_{xx}$  at  $t = 20 \Omega_i^{-1}$ , (b)  $(\nabla \cdot \mathbf{Q}_i)_{xy}$  at  $t = 7 \Omega_i^{-1}$ , (c)  $(\nabla \cdot \mathbf{Q}_e)_{yy}$  at  $t = 17.5 \Omega_i^{-1}$ .

$y = \text{const.}$ , multiplying it by  $-i \frac{k}{|k|} = -i \text{sgn}(k)$  and then Fourier transforming back to physical space. This corresponds to the Hilbert transform of the perturbed pressure. Data was taken at  $t = 17.5 \Omega_i^{-1}$  and  $y = -4.27 d_{i,0}$ . The results, compared to the actual heat flux, are plotted exemplarily (Fig. 2). Their shape is often correct but there are deviations from the heat flux data in magnitude or even sign. So the issues are similar to those of the scalar- $k$  closure, although to lesser extent.

As done before with the scalar- $k$  closure, we also compare the gradient closure to heat flux data from a Vlasov run. A comparison of magnitude suggests  $k_{0,s} = 3/d_{s,0}$  for the characteristic wave number in the new closure. This is also the value that was used for the plots in Fig. 3. Improvements are recognizable like a better representation of extrema (Fig. 3a). It has been asserted before that the scalar- $k$  closure sometimes yields bad results in the outer regions which was not the case with the original Hammett-Perkins closure. This issue has indeed been fixed using the Laplacian as can be seen in Fig. 3b and 3c. Recent efforts to couple the Vlasov equation to ten moment fluid equations (Rieke *et al.* 2015; Trost *et al.* 2017) could profit from the improvement in the outer region since that is where the fluid model would be used in a coupling scenario.

## 8. The pressure gradient closure in reconnection simulations

### 8.1. GEM

In the GEM setup the gradient fluid run is compared to both the kinetic Vlasov run and a scalar- $k$  fluid run. The respective plots can be seen in Fig. 4. Snapshots are taken at times where a similar amount of flux has reconnected since fluid simulations of Harris sheet reconnection usually have a longer onset than kinetic ones. This is measured

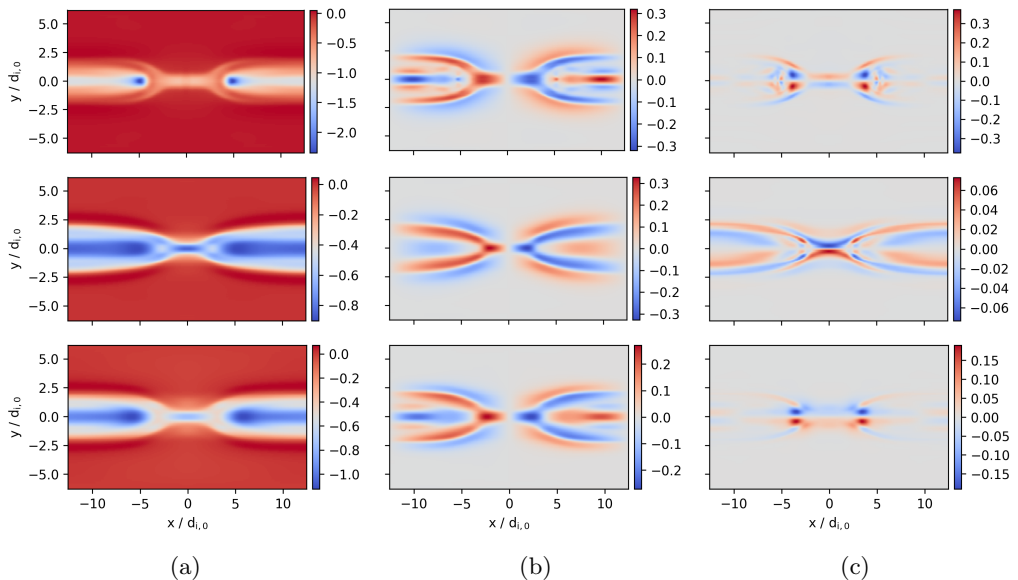


Figure 4: Vlasov run (first row), scalar- $k$  fluid run (second row) and gradient fluid run (third row). (a)  $j_z$  when  $\Psi = 1.8$ , (b)  $j_x$  when  $\Psi = 2$ , (c)  $P_{xy,e}$  when  $\Psi = 2$ .

by integrating the absolute value of the y-component of the magnetic field, i.e. the reconnected flux is  $\Psi = \int dx |B_y|/2$ .

The scalar- $k$  simulation of the GEM setup that is displayed here was computed with  $k_{0,i} = 0.3 d_{i,0}^{-1}$  and  $k_{0,e} = 5 d_{i,0}^{-1}$  which gave the best agreement with the Vlasov simulation (cf. Sec. 6). Significant improvement can be observed in the run with the gradient closure throughout all parameters. Also, time development of the gradient run is closer to the Vlasov run. Fig. 4a shows that the extremum of the current after reconnection is caught better. Details like the extrema and the changing sign in Fig. 4b in the outer areas around the x-axis that the scalar- $k$  run misses are now included. This indicates that the new closure provides a better representation of kinetic effects. Heat flux change directly influences the pressure tensor, so it is particularly interesting that the agreement with the kinetic pressure tensor has improved. In Fig. 4c an example is shown where the scalar- $k$  closure produces a result significantly different from the Vlasov run while the result from the gradient closure is very similar.

## 8.2. WHBG

Originally, the scalar- $k$  closure was tested by Wang *et al.* (2015) in the case of reconnection in a larger domain of size  $(100 \times 50) d_{i,0}$ . They compared the ten moment scalar- $k$  closure to a kinetic particle in cell (PIC) simulation and found good agreement but some issues as well. Fig. 5 shows ten moment runs of the WHBG setup with the scalar- $k$  closure on one hand and the gradient closure on the other hand with a resolution of  $2048 \times 1024$  cells. There are differences between our scalar- $k$  run and the plots by Wang *et al.* which might be attributed to the different numerical schemes used, CWENO here and discontinuous Galerkin in their case (Loverich *et al.* 2011). Despite

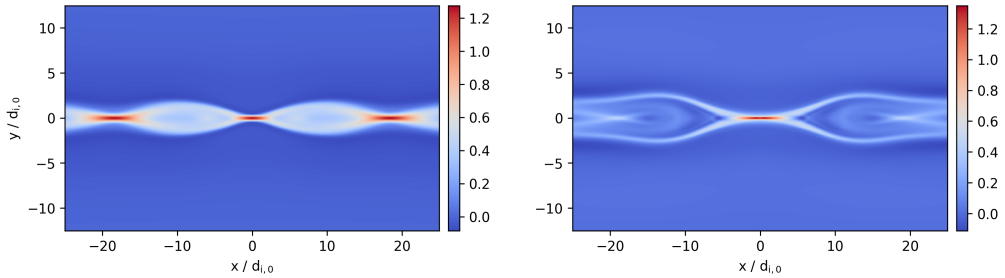


Figure 5: Scalar- $k$  closure (left) and gradient closure (right) in the WHBG setup when  $\Psi = 3$ .

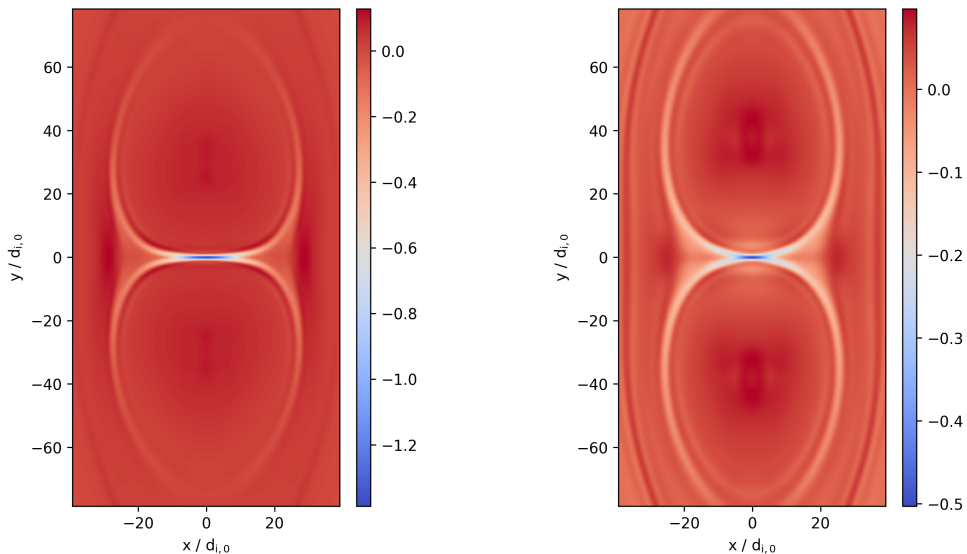


Figure 6: The island coalescence setup at  $t = t_A$  for  $\lambda = 25 d_{i,0}$ . Scalar- $k$  closure (left) and gradient closure (right).

the plasmoids that form in the scalar- $k$  simulation, time development is the same as in Wang *et al.*'s version (see the next section for further discussion). In the gradient run, however, no plasmoids form and the shape is very similar to Wang *et al.*'s PIC run. The characteristic wave numbers in the gradient closure were chosen as  $k_{0,s} = \frac{1}{3} d_{s,0}^{-1}$ .

### 8.3. Island coalescence

The coalescence of islands has been observed in space plasmas and is reported to accelerate electrons to high energies (Song *et al.* 2012). Until now no fluid or MHD model was capable of reproducing the kinetic effects in island coalescence well. Ng *et al.* (2015) found good agreement of the scalar- $k$  ten moment model with PIC runs on small spatial scales with  $k_{0,e} = 5 d_{i,0}^{-1}$ ,  $k_{0,i} = 0.3 d_{i,0}^{-1}$  as the optimal wave number values. Going to larger islands, however, average reconnection rates decreased according to  $(\lambda/d_{i,0})^{-0.2}$  whereas there was a stronger scaling of  $(\lambda/d_{i,0})^{-0.8}$  in kinetic PIC simulations (see also Stanier *et al.* (2015)). There were also further differences from kinetic simulations, e.g.

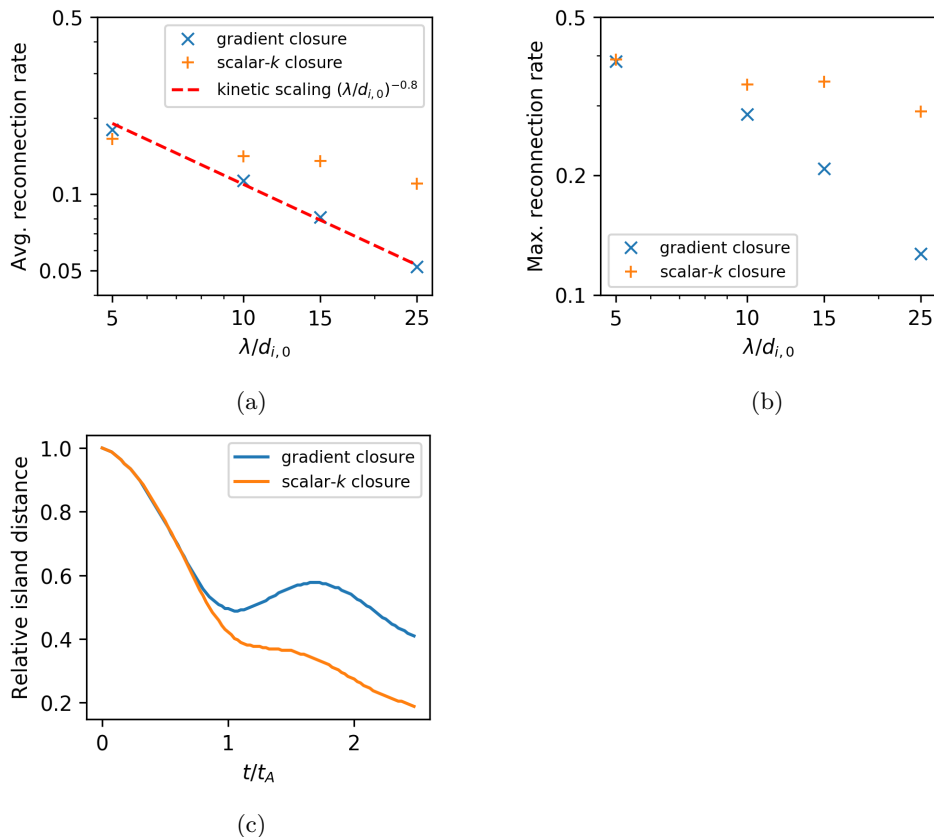


Figure 7: Coalescence of magnetic islands. (a) Scaling of the average reconnection rate with the size parameter  $\lambda$  for both closures next to the scaling found by Stanier *et al.* (2015) in kinetic PIC simulations which was  $\propto (\lambda/d_{i,0})^{-0.8}$ . (b) Scaling of the maximum reconnection rate. (c) Distance of the islands' O-points relative to their initial distance for  $\lambda = 15 d_{i,0}$ .

islands did not bounce from each other and secondary islands formed in larger systems.

Ng *et al.* (2017) proposed a global generalization (see Eq. 7.1) of the Hammett-Perkins closure to tensors and tested it in the island coalescence setup. The generalization is in Fourier space which is computationally expensive but has the advantage that no  $k_0$  needs to be chosen. It performed better than the scalar- $k$  closure concerning the average reconnection rates ( $\propto (\lambda/d_{i,0})^{-0.45}$ ) but did not approach the kinetic scaling. Scaling of maximum reconnection rate did not improve significantly and the other discrepancies mentioned above remained.

We conducted runs of the island coalescence problem with the scalar- $k$  and the gradient closure. Resolutions were chosen so that electron inertial length  $d_e$  is resolved. The results of our scalar- $k$  simulations are very similar to those of Ng *et al.* (2017) with a scaling of the average reconnection rate  $\propto (\lambda/d_{i,0})^{-0.23}$  and also matching values for the maximum reconnection rate. In our simulations no secondary islands formed though. This is particularly interesting because in the WHBG setup Wang *et al.* had no

secondary islands and we did (cf. the previous section) while here it is the other way around. Anyway, in both cases the appearance of plasmoids seems to have only minor influence on time development and reconnection rates.

Fluid simulations with the gradient closure and  $k_{0,s} = \frac{1}{2}/d_{s,0}$  show the characteristics of kinetic simulations. The average reconnection rate (average taken from 0 to  $1.5 t_A$ ) is displayed in Fig. 7a and scales as  $(\lambda/d_{i,0})^{-0.73}$  which is almost identical to the kinetic scaling. Scaling of the maximum reconnection rate is much stronger than with the scalar- $k$  closure as well (Fig. 7b). There is no formation of secondary islands. Due to the lower reconnection rates, islands now bounce as can be seen in Fig. 7c. The out-of-plane current  $j_z$  is displayed in Fig. 6 for both closures. The current sheet and the island's oval form in the gradient simulation are similar to results from kinetic simulations (see the movie in the supplemental material of Stanier *et al.* (2015)).

#### 8.4. Numerics

The Laplacian in the closure was computed explicitly by means of finite differences. Therefore, instabilities are enhanced and a smaller time step is needed. Time step restrictions increase with higher resolution. For now, this has been circumvented by subcyclng the computation of the Laplacian. Since the domain has to be split up into blocks for parallelization, and since boundaries are not exchanged in between the subcycles (for performance reasons), inaccuracies occur at these borders. Furthermore, the velocities and densities needed to compute pressure from the second moment are not updated between the subcycles, which has little influence though. A comparison of a subcycled version of the WHBG setup with one without subcyclng shows that globally there is no difference and that the approximation is acceptable when used thoughtfully. The gradient closure runs displayed in Fig. 5 and Fig. 6 were computed with 16 subcycles and a time step identical to the respective scalar- $k$  runs. A more sophisticated solution to the time step problem is left to future work.

## 9. Conclusion

Following an analysis of kinetic heat flux data, a closure to the ten moment fluid equations is presented which approximates the heat flux tensor as

$$\partial_m Q_{ijm} = -\frac{v_t}{|k_{0,s}|} \nabla^2 (P_{ij} - p\delta_{ij}) \quad (9.1)$$

with the free parameter  $k_{0,s}$  (a typical wave number) and  $p = (P_{xx} + P_{yy} + P_{zz})/3$ . Suitable values for  $k_{0,s}$  in magnetic reconnection are  $3/d_{s,0}$  in the GEM setup,  $\frac{1}{3}/d_{s,0}$  in the WHBG setup and  $\frac{1}{2}/d_{s,0}$  in island coalescence.

The derivation of Eq. 9.1 used findings of Hammett & Perkins (1990) and Wang *et al.* (2015). The approximations made were motivated by a test of the original one-dimensional Hammett-Perkins approach along magnetic field lines. The new closure was tested in three different reconnection setups and the results agreed well with kinetic Vlasov and PIC simulations in all cases. Good results were achieved in the coalescence of magnetic islands where fluid models were unsuccessful before. Including the pressure gradient is supposed to improve the modeling of kinetic effects like Landau damping so that the fluid equations can replace expensive kinetic computations. That way

simulations of large spatial scales like Earth's magnetotail become within reach.

Future work includes further investigation of the free parameter because currently it has to be determined from experiments and the comparison with kinetic simulations. The focus should be on the effect of different setups since the free parameter appears to be specific to the respective problem. Another approach would be to couple the fluid code to Vlasov computations in order to adaptively adjust the free parameter. From a technical point of view, elaborate solutions to the time step restrictions caused by the Laplacian would be desirable.

FAR appreciated the helpful discussions with Simon Lautenbach. Computations were conducted on the Davinci cluster at TP1 Plasma Research Department and on the JURECA cluster at Jülich Supercomputing Center under the project number HBO43.

#### REFERENCES

- BIRN, J., DRAKE, J. F., SHAY, M. A., ROGERS, B. N., DENTON, R. E., HESSE, M., KUZNETSOVA, M., MA, Z. W., BHATTACHARJEE, A., OTTO, A. & PRITCHETT, P. L. 2001 Geospace environmental modeling (gem) magnetic reconnection challenge. *Journal of Geophysical Research: Space Physics* **106** (A3), 3715–3719.
- CHUST, T. & BELMONT, G. 2006 Closure of fluid equations in collisionless magnetoplasmas. *Physics of Plasmas* **13** (1), 012506.
- DAUGHTON, W., ROYTERSHEYN, V., ALBRIGHT, B. J., KARIMABADI, H., YIN, L. & BOWERS, KEVIN J. 2009 Influence of coulomb collisions on the structure of reconnection layers. *Physics of Plasmas* **16** (7), 072117.
- DAUGHTON, WILLIAM, SCUDDER, JACK & KARIMABADI, HOMA 2006 Fully kinetic simulations of undriven magnetic reconnection with open boundary conditions. *Physics of Plasmas* **13** (7), 072101.
- FADEEV, V. M., KVABTSKHAVA, I. F. & KOMAROV, N. N. 1965 Self-focusing of local plasma currents. *Nuclear Fusion* **5** (3), 202.
- HAMMETT, G. W., DORLAND, W. & PERKINS, F. W. 1992 Fluid models of phase mixing, landau damping, and nonlinear gyrokinetic dynamics. *Physics of Fluids B* **4** (7), 2052–2061.
- HAMMETT, GREGORY W. & PERKINS, FRANCIS W. 1990 Fluid moment models for landau damping with application to the ion-temperature-gradient instability. *Phys. Rev. Lett.* **64**, 3019–3022.
- HARRIS, E. G. 1962 On a plasma sheath separating regions of oppositely directed magnetic field. *Il Nuovo Cimento (1955-1965)* **23** (1), 115–121.
- JOHNSON, E. ALEC & ROSSMANITH, JAMES A. 2010 Ten-moment two-fluid plasma model agrees well with pic/vlasov in gem problem. *arxiv* .
- KARIMABADI, H., DORELLI, J., ROYTERSHEYN, V., DAUGHTON, W. & CHACÓN, L. 2011 Flux pileup in collisionless magnetic reconnection: Bursty interaction of large flux ropes. *Phys. Rev. Lett.* **107**, 025002.
- LOVERICH, JOHN, HAKIM, AMMAR & SHUMLAK, URI 2011 A discontinuous galerkin method for ideal two-fluid plasma equations. *Communications in Computational Physics* **9** (2), 240268.
- NG, JONATHAN, HAKIM, AMMAR, BHATTACHARJEE, A., STANIER, ADAM & DAUGHTON, W. 2017 Simulations of anti-parallel reconnection using a nonlocal heat flux closure. *Physics of Plasmas* **24** (8), 082112, arXiv: <http://dx.doi.org/10.1063/1.4993195>.
- NG, JONATHAN, HUANG, YI-MIN, HAKIM, AMMAR, BHATTACHARJEE, A., STANIER, ADAM, DAUGHTON, WILLIAM, WANG, LIANG & GERMASCHEWSKI, KAI 2015 The island coalescence problem: Scaling of reconnection in extended fluid models including higher-order moments. *Physics of Plasmas* **22** (11), 112104.
- PASSOT, T. & SULEM, P. L. 2003 Long-alfvn-wave trains in collisionless plasmas.

- ii. a landau-fluid approach. *Physics of Plasmas* **10** (10), 3906–3913, arXiv: <http://dx.doi.org/10.1063/1.1600442>.
- RIEKE, M., TROST, T. & GRAUER, R. 2015 Coupled vlasov and two-fluid codes on gpus. *Journal of Computational Physics* **283**, 436 – 452.
- SARAZIN, Y., DIF-PRADALIER, G., ZARZOSO, D., GARBET, X., GHENDRIH, PH. & GRANDGIRARD, V. 2009 Entropy production and collisionless fluid closure. *Plasma Physics and Controlled Fusion* **51** (11), 115003.
- SCHMITZ, H. & GRAUER, R. 2006*a* Comparison of time splitting and backsubstitution methods for integrating vlasov’s equation with magnetic fields. *Comp. Phys. Comm.* **175**, 86.
- SCHMITZ, H. & GRAUER, R. 2006*b* Kinetic vlasov simulations of collisionless magnetic reconnection. *Physics of Plasmas* **13** (9), 092309.
- SONG, HONG-QIANG, CHEN, YAO, LI, GANG, KONG, XIANG-LIANG & FENG, SHI-WEI 2012 Coalescence of macroscopic magnetic islands and electron acceleration from stereo observation. *Phys. Rev. X* **2**, 021015.
- STANIER, A., DAUGHTON, W., CHACÓN, L., KARIMABADI, H., NG, J., HUANG, Y.-M., HAKIM, A. & BHATTACHARJEE, A. 2015 Role of ion kinetic physics in the interaction of magnetic flux ropes. *Phys. Rev. Lett.* **115**, 175004.
- TROST, T., LAUTENBACH, S. & GRAUER, R. 2017 Enhanced conservation properties of vlasov codes through coupling with conservative fluid models. *arxiv* .
- WANG, LIANG, HAKIM, AMMAR H., BHATTACHARJEE, A. & GERMASCHEWSKI, K. 2015 Comparison of multi-fluid moment models with particle-in-cell simulations of collisionless magnetic reconnection. *Physics of Plasmas* **22** (1), 012108.